

4.8. From top to bottom: Torque, heave position and velocity with respect to time for experiment 3

negative. Weight was changed adding on ROMEOS top, during each experiment, one diver's lead weight which reasonably does not affect the hydrodynamic derivatives but only the overall weight of the system. During all experiments the heading of the vehicle was kept constant by the action of the heading autopilot. This suggests that momentum drag due to the horizontal thrusters could be present and should be taken into account. The heave velocity has been calculated off-line processing the depth signal with a non-causal Savitzky-Golay polynomial [68] filter of fourth order with a symmetric moving window of 141 points. As only the stationary values of the velocities were needed for the identification process, these have been calculated averaging the velocity signal far from the inversion points to exclude the non stationary system response at each inversion on one side, and the last 70 samples of each constant input zone that could introduce bias in the estimated velocity, on the other. The heave motion is described with respect to a body fixed reference frame having its  $z$  axis pointing downward; indicating with  $\mathbf{w}$  the heave velocity, with  $\mathbf{F}$  the thruster applied force, with  $\mathbf{W}$  the weight and buoyancy force, with  $m$  the sum of inertial and added mass, with  $k_w$  and  $k_{w|w|}$  the linear and quadratic drag coefficients according to subsection (4.2.1) the standard heave model is:

$$m \dot{\mathbf{w}} = -k_w \mathbf{w} - k_{w|w|} \mathbf{w}|\mathbf{w}| + \mathbf{F} + \mathbf{W} \quad (4.15)$$

where  $\mathbf{w}$  and  $\mathbf{F}$  are assumed to be known far from the inversion points, i.e., in stationary conditions  $\dot{\mathbf{w}} = 0$ . Equation (4.15) is linear in the unknown parameters and, calling  $\mathbf{e}_z$  the  $z$  axis unit vector, when  $\dot{\mathbf{w}} = 0$  it can be written in the more convenient form  $\mathbf{y}_s = H_s \boldsymbol{\theta}_s + \boldsymbol{\varepsilon}_s$  being  $\boldsymbol{\theta}_s = [k_w \ k_w|\mathbf{w}| \ (\mathbf{W}^T \mathbf{e}_z)]^T$  the parameter vector,  $\mathbf{y}_s =$

$$[\mathbf{F}_1^T \mathbf{e}_z \ \mathbf{F}_2^T \mathbf{e}_z \ \cdots \ \mathbf{F}_m^T \mathbf{e}_z]^T \text{ the measurement vector, } H_s = \begin{bmatrix} \mathbf{w}_1^T \mathbf{e}_z & \mathbf{w}_1^T \mathbf{e}_z |\mathbf{w}_1| & -1 & \\ \mathbf{w}_2^T \mathbf{e}_z & \mathbf{w}_2^T \mathbf{e}_z |\mathbf{w}_2| & -1 & \\ \vdots & \vdots & \vdots & \\ \mathbf{w}_m^T \mathbf{e}_z & \mathbf{w}_m^T \mathbf{e}_z |\mathbf{w}_m| & -1 & \end{bmatrix}$$

the regression matrix and  $\boldsymbol{\varepsilon}_s$  the measurement noise. Each stationary velocity  $\mathbf{w}_i$  is calculated as described above. As shown in the pictures in figure (4.1) the vertical propellers of the ROME0 ROV are at the very top of the frame in order to avoid large turbulence next to the sea bottom that could limit visibility in the presence of sand or dust. As a consequence when the vertical thrusters push upwards the water flow out of the propellers interferes with the vehicles structure. It is then reasonable to assume that when the thrusters' force is directed upwards the efficiency of the vertical thrusters will be affected by a propeller-hull interaction virtually absent when the force is directed downwards. This suggests to modify equation (4.15) with the introduction of an efficiency parameter  $\eta$  such that in stationary conditions the vehicles model can be written as

$$\begin{aligned} \eta \mathbf{F} &= k_w \mathbf{w} + k_{w|\mathbf{w}|} \mathbf{w}|\mathbf{w}| - \mathbf{W} \\ &\begin{cases} \eta = 1 \ \forall \ \mathbf{F}^T \mathbf{e}_z \geq 0 \\ \eta < 1 \ \forall \ \mathbf{F}^T \mathbf{e}_z < 0 \end{cases} \end{aligned} \quad (4.16)$$

( $\mathbf{e}_z$  is the  $z$ -axis unit vector pointing downwards) which will be called *eta* model in the sequel. Indicating with the subscripts  $d$  and  $u$  forces and velocities in the downward and upward directions, the regression form of equation (4.16) can be written as

$$\mathbf{y}_\eta = H_\eta \boldsymbol{\theta}_\eta + \boldsymbol{\varepsilon}_\eta$$

$$\mathbf{y}_\eta = [\mathbf{F}_{d1}^T \mathbf{e}_z \ \mathbf{F}_{d2}^T \mathbf{e}_z \ \cdots \ \mathbf{F}_{dm}^T \mathbf{e}_z \ 0 \ 0 \ \cdots \ 0]^T \in \Re^{(m+p) \times 1}$$

$$H_\eta = \begin{bmatrix} \mathbf{w}_{d1}^T \mathbf{e}_z & \mathbf{w}_{d1}^T \mathbf{e}_z |\mathbf{w}_{d1}| & -1 & 0 \\ \vdots & \vdots & \vdots & \vdots \\ \mathbf{w}_{dm}^T \mathbf{e}_z & \mathbf{w}_{dm}^T \mathbf{e}_z |\mathbf{w}_{dm}| & -1 & 0 \\ -\mathbf{w}_{u1}^T \mathbf{e}_z & -\mathbf{w}_{u1}^T \mathbf{e}_z |\mathbf{w}_{u1}| & 1 & \mathbf{F}_{u1}^T \mathbf{e}_z \\ \vdots & \vdots & \vdots & \vdots \\ -\mathbf{w}_{up}^T \mathbf{e}_z & -\mathbf{w}_{up}^T \mathbf{e}_z |\mathbf{w}_{up}| & 1 & \mathbf{F}_{up}^T \mathbf{e}_z \end{bmatrix} = \begin{bmatrix} w_{d1} & w_{d1}^2 & -1 & 0 \\ \vdots & \vdots & \vdots & \vdots \\ w_{dm} & w_{dm}^2 & -1 & 0 \\ w_{u1} & w_{u1}^2 & 1 & -F_{u1} \\ \vdots & \vdots & \vdots & \vdots \\ w_{up} & w_{up}^2 & 1 & -F_{up} \end{bmatrix}$$

$$\boldsymbol{\theta}_\eta = [k_{\mathbf{w}} k_{\mathbf{w}|\mathbf{w}}| (\mathbf{W}^T \mathbf{e}_z) \eta]^T$$

being  $w$  and  $F$  the norms of vectors  $\mathbf{w}$  and  $\mathbf{F}$  following the standard notation  $a \triangleq \|\mathbf{a}\|$ . The third and last considered model takes explicitly into account the momentum drag discussed in section (3.3.1). As during all the experiments the heading of the vehicle was kept constant with the horizontal thrusters, their effect on the heave drag may be modelled by  $\mathbf{F}_{md} = -\alpha n_h \mathbf{w}$  where  $n_h$  is the mean propeller revolution rate modulus of the four horizontal thrusters,  $\alpha$  is an unknown constant parameter and  $\mathbf{w}$  the heave velocity. Adding  $\mathbf{F}_{md}$  in equation (4.16) gives rise to the *eta-md* model which can be written in regression form as

$$\eta \mathbf{F} = k_{\mathbf{w}} \mathbf{w} + k_{\mathbf{w}|\mathbf{w}} |\mathbf{w}|\mathbf{w}| - \mathbf{W} + \alpha n_h \mathbf{w} : \begin{cases} \eta = 1 \forall \mathbf{F}^T \mathbf{e}_z \geq 0 \\ \eta < 1 \forall \mathbf{F}^T \mathbf{e}_z < 0 \end{cases}$$

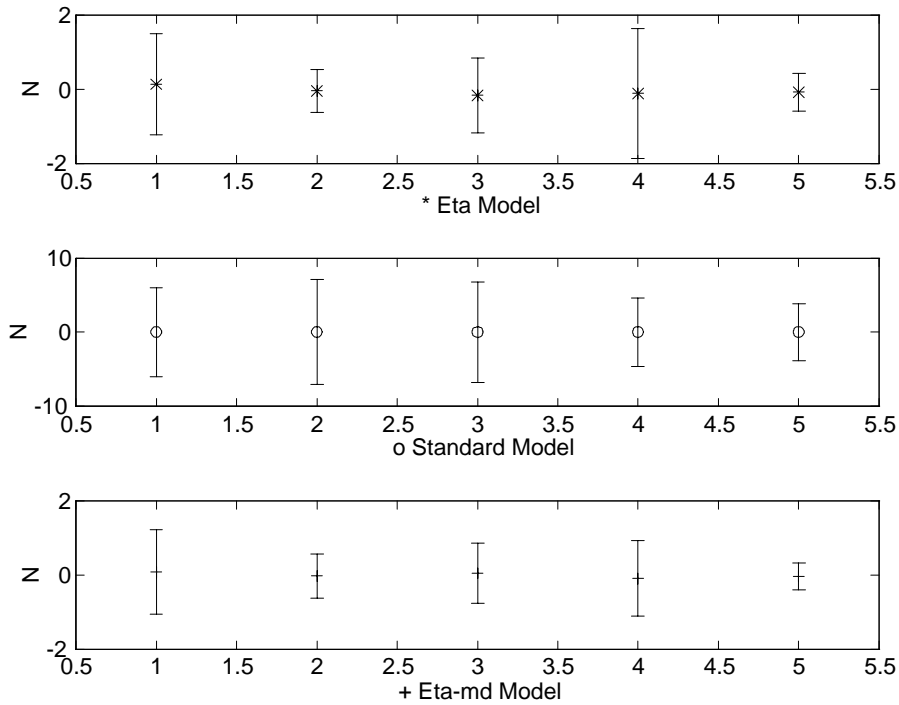
$$\mathbf{y}_{md} = H_{md} \boldsymbol{\theta}_{md} + \boldsymbol{\varepsilon}_{md}$$

$$\mathbf{y}_{md} = [\mathbf{F}_{d1}^T \mathbf{e}_z \mathbf{F}_{d2}^T \mathbf{e}_z \cdots \mathbf{F}_{dm}^T \mathbf{e}_z \ 0 \ 0 \ \cdots \ 0]^T \in R^{(m+p) \times 1}$$

$$H_{md} = \begin{bmatrix} \mathbf{w}_{d1}^T \mathbf{e}_z & \mathbf{w}_{d1}^T \mathbf{e}_z |\mathbf{w}_{d1}| & -1 & 0 & n_{h1} \mathbf{w}_{d1}^T \mathbf{e}_z \\ \vdots & \vdots & \vdots & \vdots & \vdots \\ \mathbf{w}_{dm}^T \mathbf{e}_z & \mathbf{w}_{dm}^T \mathbf{e}_z |\mathbf{w}_{dm}| & -1 & 0 & n_{hm} \mathbf{w}_{dm}^T \mathbf{e}_z \\ -\mathbf{w}_{u1}^T \mathbf{e}_z & -\mathbf{w}_{u1}^T \mathbf{e}_z |\mathbf{w}_{u1}| & 1 & \mathbf{F}_{u1}^T \mathbf{e}_z & -n_{u1} \mathbf{w}_{u1}^T \mathbf{e}_z \\ \vdots & \vdots & \vdots & \vdots & \vdots \\ -\mathbf{w}_{up}^T \mathbf{e}_z & -\mathbf{w}_{up}^T \mathbf{e}_z |\mathbf{w}_{up}| & 1 & \mathbf{F}_{up}^T \mathbf{e}_z & -n_{up} \mathbf{w}_{up}^T \mathbf{e}_z \end{bmatrix} = \begin{bmatrix} w_{d1} & w_{d1}^2 & -1 & 0 & n_{h1} w_{d1} \\ \vdots & \vdots & \vdots & \vdots & \vdots \\ w_{dm} & w_{dm}^2 & -1 & 0 & n_{hm} w_{dm} \\ w_{u1} & w_{u1}^2 & 1 & -F_{u1} & n_{u1} w_{u1} \\ \vdots & \vdots & \vdots & \vdots & \vdots \\ w_{up} & w_{up}^2 & 1 & -F_{up} & n_{up} w_{up} \end{bmatrix}$$

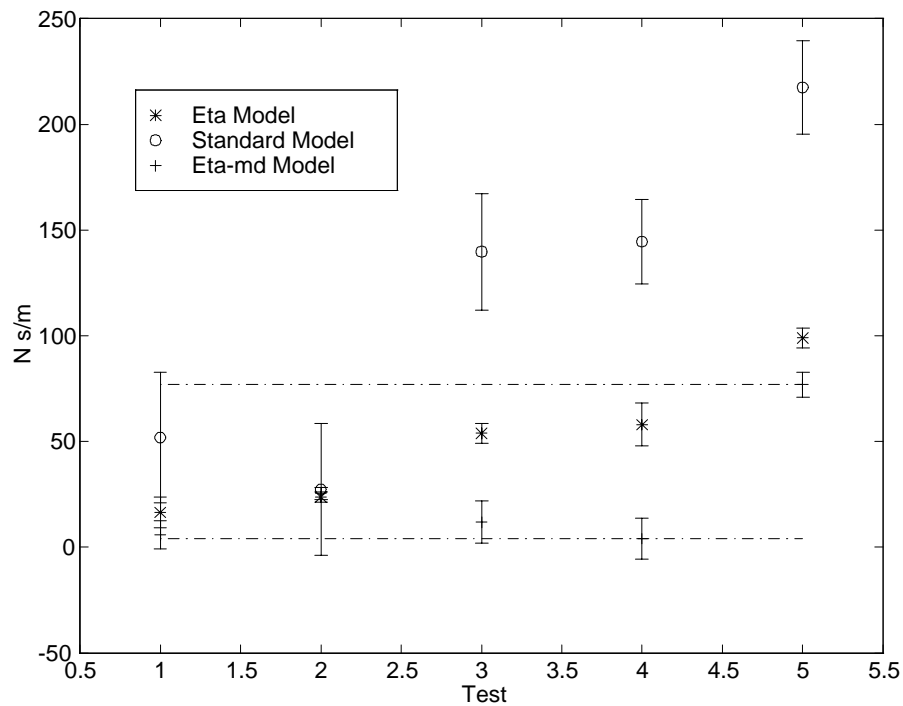
$$\boldsymbol{\theta}_{md} = [k_{\mathbf{w}} k_{\mathbf{w}|\mathbf{w}}| (\mathbf{W}^T \mathbf{e}_z) \eta \alpha]^T$$

Typical values of  $m$  and  $p$  range from 4 to 7. The identification of the above models has been performed by the standard least squares technique described in the previous section. In particular indicating with  $\mathbf{y} = H\boldsymbol{\theta} + \boldsymbol{\varepsilon}$  the generic heave model, the covariance matrix  $\Sigma$  of the noise vectors  $\boldsymbol{\varepsilon}$  is considered unknown as the measurement vector  $\mathbf{y}$  is actually calculated through another identified model. Assuming  $\Sigma = \sigma_\varepsilon^2 I$  being  $\sigma_\varepsilon$  an unknown constant and  $I$  the identity matrix equations (4.5), (4.6) and (4.12) may be applied. All the parameter values and relative standard deviations presented in

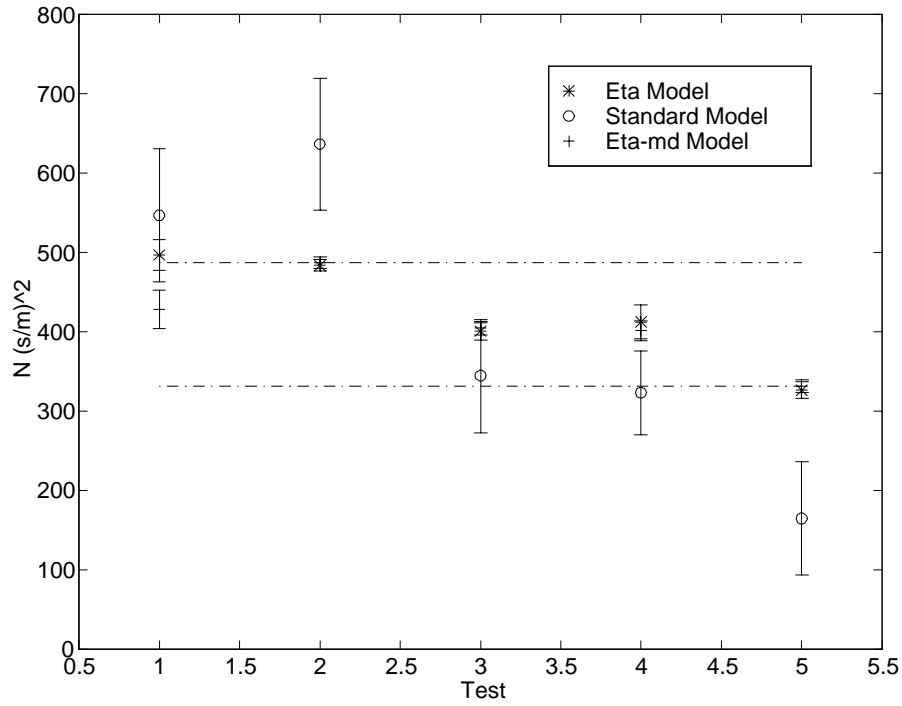
4.9. Model residuals ( $N$ ) and relative estimated standard deviation for the 5 experiments

following tables and figures have been calculated respectively as  $\hat{\theta}_{LS}$  given by equation (4.5), and the square root of the principal diagonal of matrix  $(H^T H)^{-1} \hat{\sigma}_\varepsilon^2$ , i.e.  $\hat{\sigma}_\theta = \sqrt{\text{diag}((H^T H)^{-1} \hat{\sigma}_\varepsilon^2)}$  being  $\hat{\sigma}_\varepsilon^2$  given by equation (4.12). As shown in figure (4.9) all the models perform well as far as the mean value of the residuals  $\mathbf{y} - H\hat{\theta}$  is concerned, but indeed the estimated standard deviation  $\hat{\sigma}_\varepsilon$  of the standard model residuals is from 3 to 10 times larger than for the eta or eta-md models. In figures (4.10) and (4.11) the linear and quadratic drag coefficients are plotted for the different models and experiments. The extremum values of the coefficients relative to the eta-md model, which has the smallest variation on the 5 tests with respect to the other two models, are reported by dashed lines. The scattered nature of the linear and quadratic drag coefficients shown in figures (4.10) and (4.11) for the standard model suggests a mismodelling error which is partially corrected in the other models that predict much more stable values of  $k_w$  and  $k_w|w|$ . In figure (4.12) the buoyancy force estimate for the different models is reported. Notice that while the eta-md and eta models are in perfect agreement on  $\mathbf{W}$ 's estimate, the standard model is affected by a bias on  $\mathbf{W}$  such that the vehicles results positively buoyant in all 5 tests, which is false<sup>3</sup>. This behaviour of

<sup>3</sup> The vehicle was neutrally buoyant during experiment 3, positive during experiments 1 and 2 and negative during experiments 4 and 5.



4.10. Linear drag coefficient  $k_w(Ns/m)$  for the three models in the five experiments. The dashed lines show the limits of the  $k_w$  eta-md estimate on the 5 experiments. The ranges of the other two models are larger.

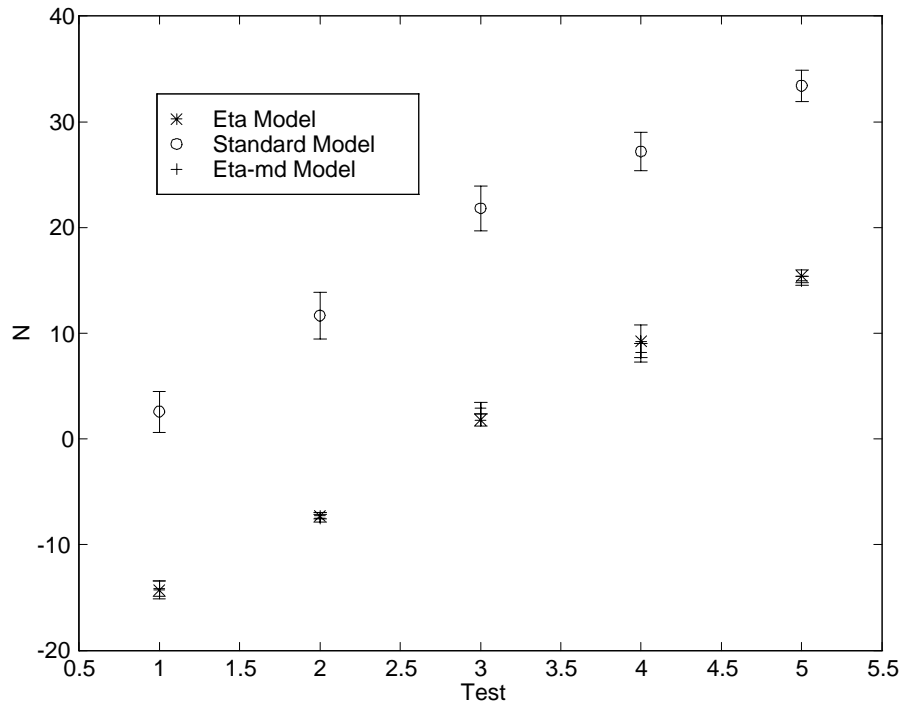


4.11. Quadratic drag coefficient  $k_{w|w|}$  ( $N s^2/m^2$ ) for the three models in the five experiments. The dashed lines show the limit of the  $k_{w|w|}$  eta-md estimate on the 5 experiments. The ranges of the other two models are larger.

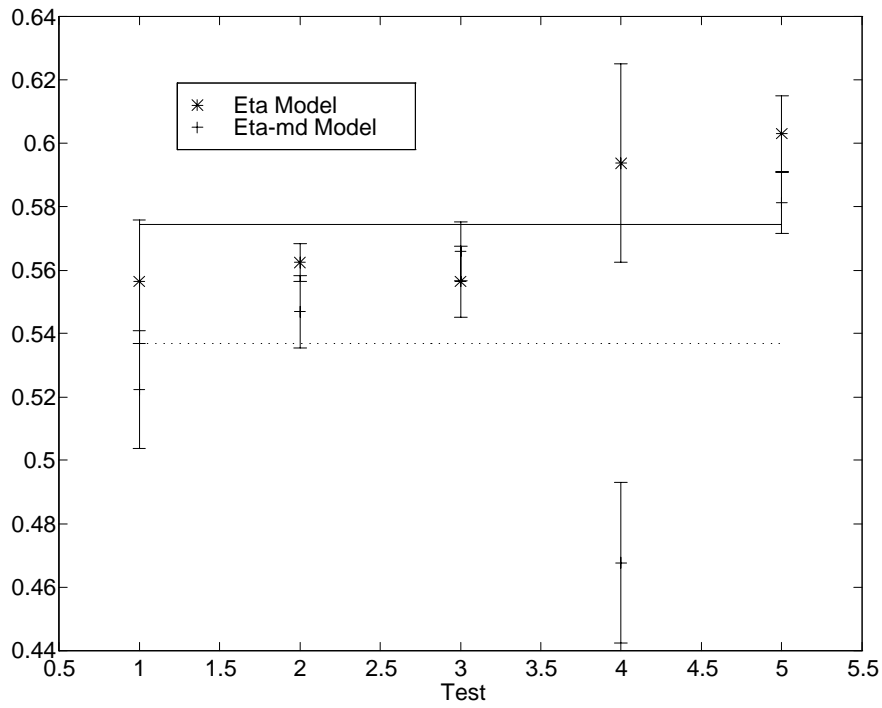
the standard model is due to the fact that neglecting the propeller-hull interaction, the standard model over-estimates the applied upward force and tries thus to compensate it with a large weight. Table I reports the maximum and minimum percentile relative error  $\frac{\Delta \hat{\theta}}{\hat{\theta}} \triangleq 100 \frac{\hat{\sigma}_{\theta}}{|\hat{\theta}|}$  of each parameter, for the three suggested models on the 5 tests. Both the estimate of the parameter and its standard deviation have been calculated as described above.

Table I		Standard	Eta	Eta-md
Max	$\frac{\Delta k_w}{k_w}$	228 %	87.2 %	475.1 %
Min	$\frac{\Delta k_w}{k_w}$	20.3 %	9.5 %	15.4 %
Max	$\frac{\Delta k_w  w }{k_w  w }$	86.9 %	10.3 %	11.2 %
Min	$\frac{\Delta k_w  w }{k_w  w }$	26.2 %	2.9 %	3.1 %
Max	$\frac{\Delta W}{W}$	151 %	66.4 %	37.4 %
Min	$\frac{\Delta W}{W}$	8.8 %	7.6 %	5.7 %
Max	$\frac{\Delta \eta}{\eta}$	/	10.5 %	10.9 %
Min	$\frac{\Delta \eta}{\eta}$	/	2.1 %	3.3 %
Max	$\frac{\Delta \alpha}{\alpha}$	/	/	125.7 %
Min	$\frac{\Delta \alpha}{\alpha}$	/	/	28 %

Table I shows that the eta model predicts the most stable parameter values of the three. The extremely imprecise estimates of the momentum drag ( $\hat{\alpha}$  of test 2 is negative!) and linear drag parameters in the eta-md model indicate that the first and last columns of the regression matrix  $H_{md}$  must share large parallel components. This is due to the fact that the modulus of the revolution rate of the horizontal thrusters  $n_h$  is very similar at the different speed regimes considered. Moreover, the poor performance of the eta-md model is clearly shown in figure (4.13) by the very scattered estimate of  $\eta$  on the five tests as compared to the eta model. The plane and dashed lines in figure (4.13) represent the mean value of  $\eta$  according to the eta and eta-md models. Concluding, the results reported in Table I and in the above plots suggest that the best model among the three is the eta model. This means that during common slow motion heave maneuvers of the ROMEO open frame ROV momentum drag forces (3.3.1) due to the propeller revolution rate of the horizontal thrusters can be modelled by the standard linear and quadratic drag forces. On the contrary propeller hull interactions are relevant and need to be modeled separately by an efficiency parameter. The above reported experimental results show that the loss of efficiency due to the propeller hull interaction in the heave direction is more then 40% ( $\eta_{md} = 0.57$ ). The numerical values of the estimated parameters and



4.12. Buoyancy force  $W(N)$  estimate for the three models in the five tests.



4.13. Efficiency  $\eta$  parameter estimate. The solid and dashed lines are the mean values of  $\eta$  according to the eta and eta-md models.

their standard deviation for the three models are reported in the following:

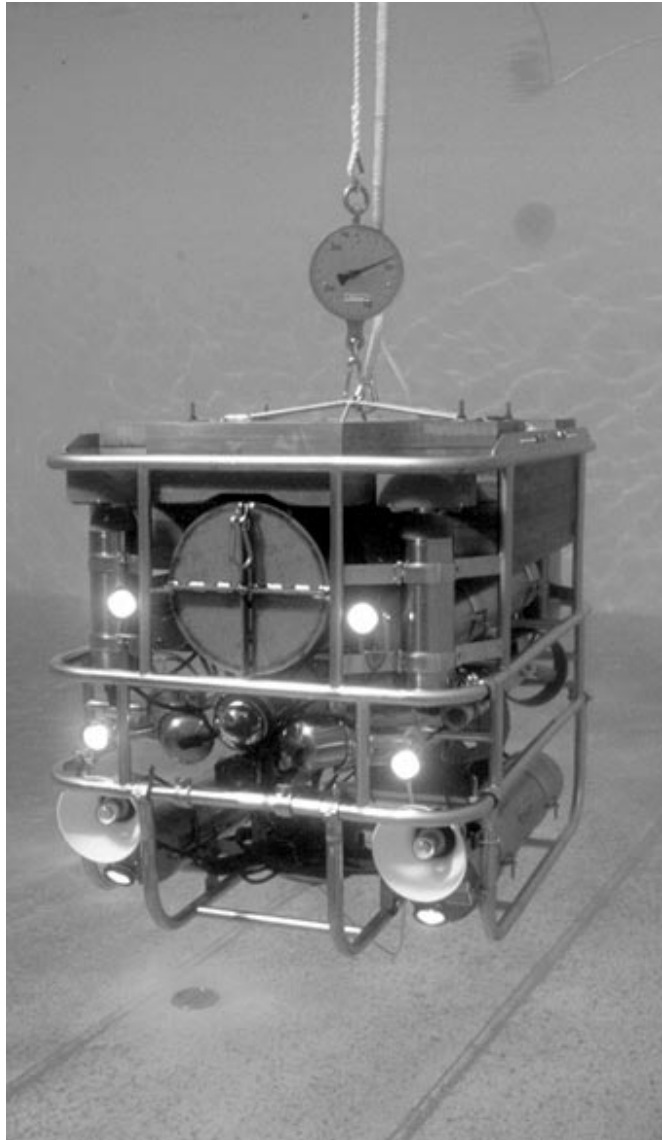
Model type	Parameter values	
Eta	$\begin{cases} k_w = & (50 \pm 12) \text{ N s/m} \\ k_{w w } = & (424 \pm 28) \text{ N s}^2/\text{m}^2 \\ \eta = & 0.57 \pm 0.03 \end{cases}$	
Eta-md	$\begin{cases} k_w = & (25 \pm 14) \text{ N s/m} \\ k_{w w } = & (411 \pm 24) \text{ N s}^2/\text{m}^2 \\ \eta = & 0.54 \pm 0.03 \\ \alpha = & 15 \pm 8 \end{cases}$	(4.17)
Standard	$\begin{cases} k_w = & (116 \pm 53) \text{ N s/m} \\ k_{w w } = & (403 \pm 145) \text{ N s}^2/\text{m}^2 \end{cases}$	

At last notice that the value of the eta model heave efficiency parameter estimated by the above described dynamic tests is remarkably similar to the value that has been measured by static tests performed in a swimming pool: ROMEO has been fixed to a dynamometer as shown in figures (4.14) (4.15) and the maximum heave force has been measured in both the positive and negative vertical directions. Figures (4.16) and (4.17) show a zoomed view of the dynamometer showing that the maximum vertical force in the downward direction is almost double then in the upwards one even in static conditions. Indeed this result validates the developed dynamic model.

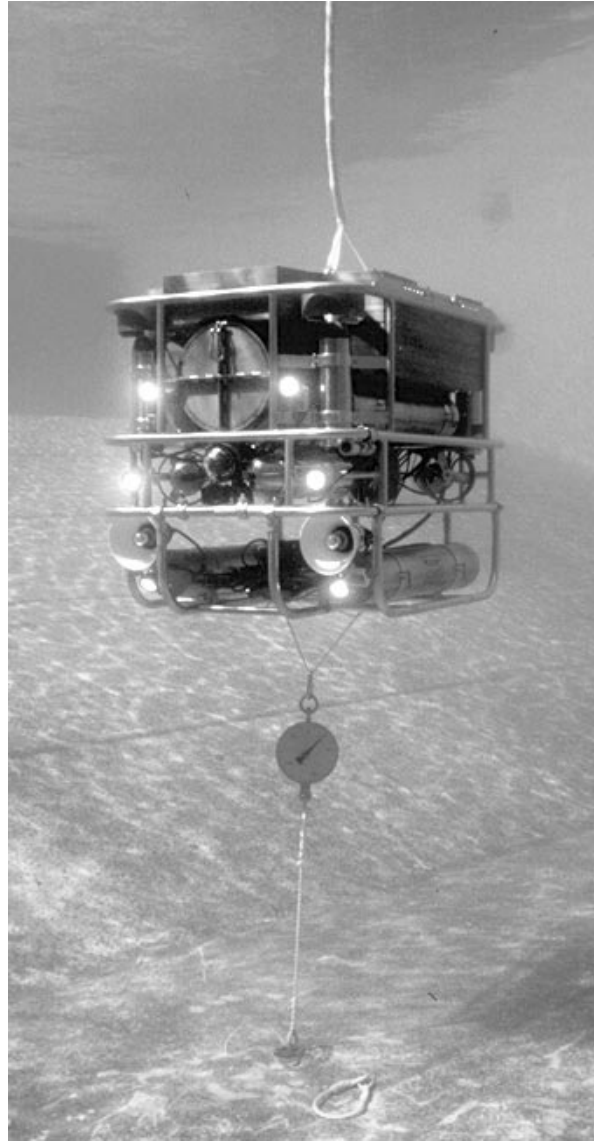
#### 4.2.5 Yaw model identification

As far as the yaw axis identification is concerned two type of experiments are analyzed. They will be called type A and B. The first consists of constant applied torque by all four horizontal thrusters, the second in constant applied torque by only two horizontal thrusters on the vehicles diagonal. With these kind of tests the loss of thruster efficiency, with respect to the thrust tunnel measured value, due to propeller hull and propeller-propeller interactions, can be estimated. The vehicle performed about one complete circle at each torque value. The angular position measured by a Watson inertial sensor and a Kvh compass has been logged (about 500 points per trial, 10Hz sampling frequency). The constant yaw rate has been evaluated by least squares (LS) on the part of signal going from 8s after the beginning of the constant torque (to avoid the transient) to its end. For the yaw rate  $\dot{\psi}$  estimate the following kinematic model has been assumed

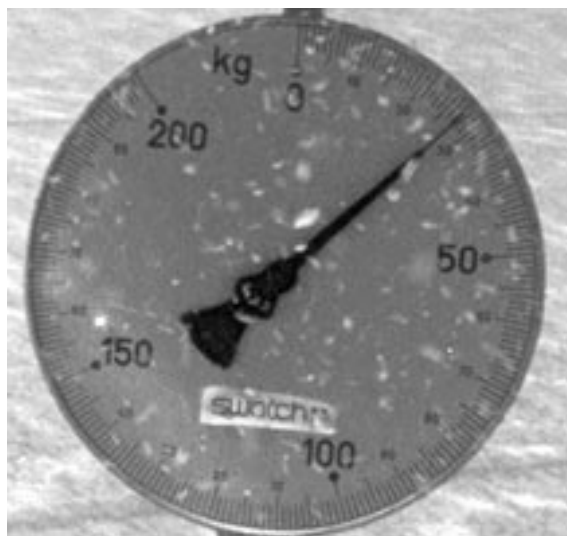
$$\mathbf{y}(t) = \dot{\psi} t + \psi_0 + \boldsymbol{\varepsilon} = \mathbf{H} \boldsymbol{\theta} + \boldsymbol{\varepsilon} \quad (4.18)$$



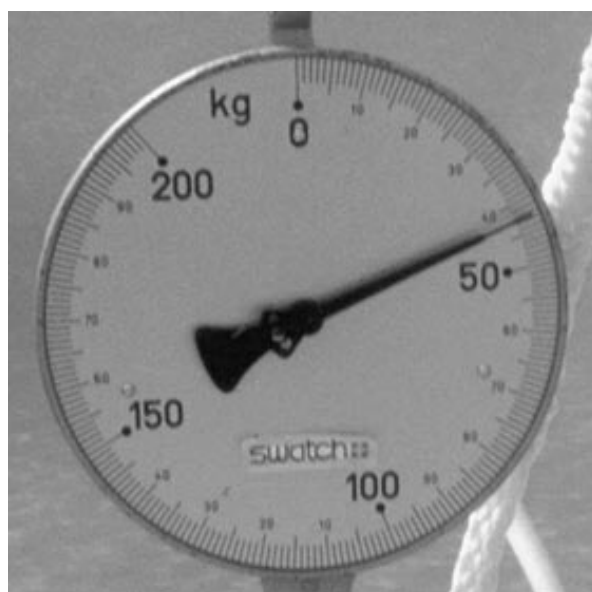
4.14. Maximum static downward thrust



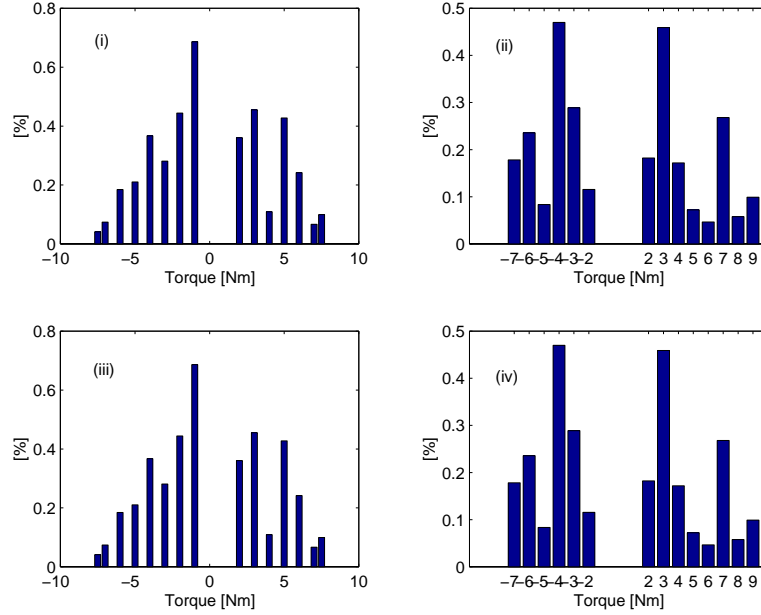
4.15. Maximum upward thrust.



4.16.Zoom of the dynamometer in the static maximum upward thrust



4.17.Zoom of the dynamometer in the static maximum downward thrust



4.18. Percentile yaw rate error for Kvh measurements experiments A (i), B (ii), and for Watson measurements experiments A (iii), B (iv).

$$H \triangleq \begin{bmatrix} t_0 & 1 \\ \vdots & \vdots \\ t_f & 1 \end{bmatrix}; \boldsymbol{\theta} \triangleq [\dot{\psi} \ \psi_0]^T; \boldsymbol{\varepsilon} \triangleq \text{noise}$$

As the variance of the noise  $\boldsymbol{\varepsilon}$  is unknown, the standard LS solution rather than the WLS one, is calculated to estimate the parameter vector

$$\hat{\boldsymbol{\theta}} = (H^T H)^{-1} H^T \mathbf{y}$$

and the  $\boldsymbol{\varepsilon}$  noise and  $\hat{\boldsymbol{\theta}}$  parameter variances  $\sigma^2$  and  $\sigma_{\hat{\boldsymbol{\theta}}}^2$  are estimated (4.12) (4.6) as

$$\begin{aligned} \hat{\sigma}^2 &= ((\mathbf{y} - H\hat{\boldsymbol{\theta}})^T (\mathbf{y} - H\hat{\boldsymbol{\theta}})) / (\dim(\mathbf{y}) - \dim(\boldsymbol{\theta})) \\ \hat{\sigma}_{\hat{\boldsymbol{\theta}}}^2 &= \text{diag}((H^T H)^{-1} \hat{\sigma}^2) \end{aligned}$$

The percentile yaw rate estimated error calculated as  $100 \frac{\hat{\sigma}_{\hat{\boldsymbol{\theta}}}}{|\hat{\boldsymbol{\theta}}|}$  for experiment A and B for both Kvh and Watson sensors is extremely small for every trial, as shown in figure (4.18) This proves that the yaw acceleration was indeed negligible during the experimental trials and that the estimated constant yawrate is very precise. Notice that the considered input torques have been chosen to match the typical operating yaw rate range

( $\sim [-10 \text{ deg/s}, 10 \text{ deg/s}]$ ).

The data of experiment A and B has been fitted with four models derived from the general equation (4.13). They will be denoted as: LQB (linear drag, quadratic drag, bias term), LQNB (linear & quadratic drag and no bias term), LB (linear drag and bias), LNB (linear drag and no bias) for the positive direction, the negative ones and putting positive and negative direction together.

$$\begin{aligned} \tau &= k_r \dot{\psi} + k_{r|r} |\dot{\psi}| \dot{\psi} + b && \text{LQB Model} \\ \tau &= k_r \dot{\psi} + k_{r|r} |\dot{\psi}| \dot{\psi} && \text{LQNB Model} \\ \tau &= k_r \dot{\psi} + b && \text{LB Model} \\ \tau &= k_r \dot{\psi} && \text{LNB Model} \end{aligned}$$

The results of the LS fits for both the Kvh and Watson sensors are reported in the following tables:

Exp. A + & - dir	Watson					
Model	LQB +	LB +	LQB -	LB -	LNB -	LNB +
$k_r$ [Nm/s/rad]	-1.28	42.613	41.458	33.25	37.498	47.035
$k_{r r}$ [Nm/s <sup>2</sup> /rad <sup>2</sup> ]	241.42	-	-35.32	-	-	-
$b$ [Nm]	2.05	0.54	-0.3	-0.63	-	-
$100 \frac{\sigma_{k_r}}{ k_r }$ [%]	2066	12.3	41.9	12.7	5.7	4.2
$100 \frac{\sigma_{k_{r r}}}{ k_{r r} }$ [%]	59.43	-	204	-	-	-
$100 \frac{\sigma_b}{ b }$ [%]	50.25	109.4	303	87	-	-
$J_{LS}$ [(Nm) <sup>2</sup> ]	1.0374	1.7717	3.2592	3.4151	4.1661	2.0681
$\nu$ DOF	4	5	5	6	7	6

Exp. A + & - dir	Kvh					
Model	LQB +	LB +	LQB -	LB -	LNB -	LNB +
$k_r$ [Nm/s/rad]	1	40.41	42.73	32.83	38.966	42.572
$k_{r r}$ [Nm/s <sup>2</sup> /rad <sup>2</sup> ]	191.6	-	-44.38	-	-	-
$b$ [Nm]	1.89	0.29	-0.53	-0.90	-	-
$100 \frac{\sigma_{k_r}}{ k_r }$ [%]	1932	10	33.4	11.26	5.75	3.3
$100 \frac{\sigma_{k_{r r}}}{ k_{r r} }$ [%]	48.4	-	138.7	-	-	-
$100 \frac{\sigma_b}{ b }$ [%]	46	174.3	131.8	51.7	-	-
$J_{LS}$ [(Nm) <sup>2</sup> ]	0.58555	1.2105	2.4789	2.7367	4.4423	1.2902
$\nu$ DOF	4	5	5	6	7	6

Exp. A	Watson			
Model	LQB	LQNB	LB	LNB
$k_r$ [ $Nms/rad$ ]	51.723	54.09	41.623	41.22
$k_{r r}$ [ $Nms^2/rad^2$ ]	-66.25	-83.81	-	-
$b$ [ $Nm$ ]	0.38	-	0.47	-
$100 \frac{\sigma_{k_r}}{ k_r }$ [%]	10.85	11.27	3.96	4.56
$100 \frac{\sigma_{k_{r r}}}{ k_{r r} }$ [%]	53.5	45.55	-	-
$100 \frac{\sigma_b}{ b }$ [%]	50	-	42.8	-
$J_{LS}$ [ $(Nm)^2$ ]	6.0436	8.0827	7.8032	11.08
$\nu$ $DOF$	12	13	13	14

Exp. A	Kvh			
Model	LQB	LQNB	LB	LNB
$k_r$ [ $Nms/rad$ ]	50.59	50.77	40.64	40.62
$k_{r r}$ [ $Nms^2/rad^2$ ]	-63.86	-65.12	-	-
$b$ [ $Nm$ ]	0.048	-	0.092	-
$100 \frac{\sigma_{k_r}}{ k_r }$ [%]	10.26	9.79	3.56	3.47
$100 \frac{\sigma_{k_{r r}}}{ k_{r r} }$ [%]	50.52	47.34	-	-
$100 \frac{\sigma_b}{ b }$ [%]	341.8	-	197.11	-
$J_{LS}$ [ $(Nm)^2$ ]	4.7945	4.8287	6.3599	6.4859
$\nu$ $DOF$	12	13	13	14

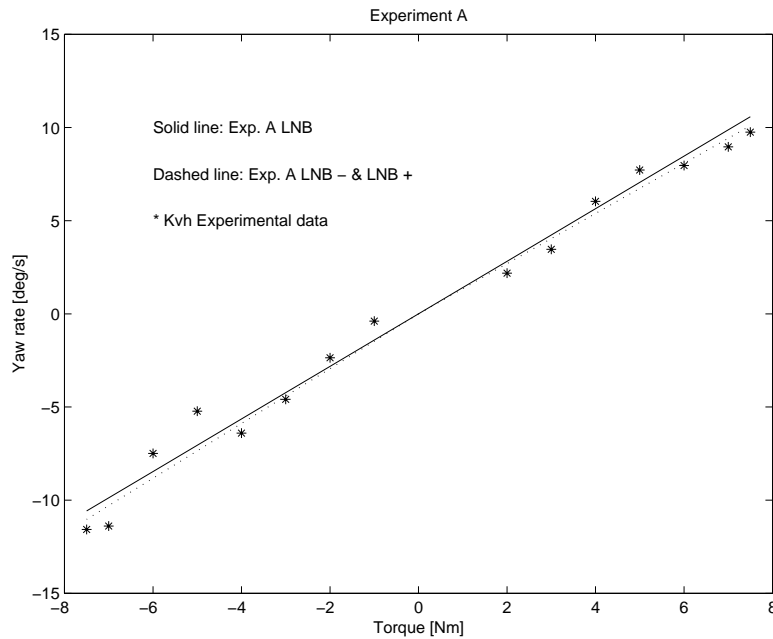
Exp. B + & - dir	Watson			
Model	LQB +	LB +	LQB -	LB -
$k_r$ [ $Nms/rad$ ]	33.042	45.62	-11.04	35.52
$k_{r r}$ [ $Nms^2/rad^2$ ]	41.64	-	223.04	-
$b$ [ $Nm$ ]	-0.73	-1.58	-2.53	-0.57
$100 \frac{\sigma_{k_r}}{ k_r }$ [%]	87.26	9.92	334	18.92
$100 \frac{\sigma_{k_{r r}}}{ k_{r r} }$ [%]	226	-	78	-
$100 \frac{\sigma_b}{ b }$ [%]	286	46.65	-67	142
$J_{LS}$ [ $(Nm)^2$ ]	2.2525	2.3408	1.4136	2.1917
$\nu$ $DOF$	5	6	3	4

Exp. B + & - dir	Kvh			
	LQB +	LB +	LQB -	LB -
Model				
$k_r$ [ $Nms/rad$ ]	21.36	42	0.44	34.17
$k_{r r}$ [ $Nms^2/rad^2$ ]	64.12	-	167.24	-
$b$ [ $Nm$ ]	-0.0092	-1.49	-2.22	-0.9
$100 \frac{\sigma_{k_r}}{ k_r }$ [%]	158.89	11.04	6404	16.32
$100 \frac{\sigma_{k_{r r}}}{ k_{r r} }$ [%]	162.77	-	81.8	-
$100 \frac{\sigma_b}{ b }$ [%]	27754	54.3	55.76	71.39
$J_{LS}$ [ $(Nm)^2$ ]	2.6594	2.8602	1.1241	1.68
$\nu$ $DOF$	5	6	3	4

Exp. B	Watson			
	LQB	LQNB	LB	LNB
Model				
$k_r$ [ $Nms/rad$ ]	29.34	32.51	38.08	37.39
$k_{r r}$ [ $Nms^2/rad^2$ ]	52.58	28.66	-	-
$b$ [ $Nm$ ]	-0.47	-	-0.35	-
$100 \frac{\sigma_{k_r}}{ k_r }$ [%]	16.86	17.62	3.48	3.69
$100 \frac{\sigma_{k_{r r}}}{ k_{r r} }$ [%]	54.95	114	-	-
$100 \frac{\sigma_b}{ b }$ [%]	40.1	-	54.53	-
$J_{LS}$ [ $(Nm)^2$ ]	4.4195	6.9175	5.75	7.3617
$\nu$ $DOF$	11	12	12	13

Exp. B	Kvh			
	LQB	LQNB	LB	LNB
Model				
$k_r$ [ $Nms/rad$ ]	30.57	35.93	37.08	35.7
$k_{r r}$ [ $Nms^2/rad^2$ ]	37.08	-1.26	-	-
$b$ [ $Nm$ ]	-0.75	-	-0.64	-
$100 \frac{\sigma_{k_r}}{ k_r }$ [%]	15.23	18.16	3.31	4.38
$100 \frac{\sigma_{k_{r r}}}{ k_{r r} }$ [%]	69.25	2751	-	-
$100 \frac{\sigma_b}{ b }$ [%]	25.94	-	29.21	-
$J_{LS}$ [ $(Nm)^2$ ]	4.384	10.308	5.2151	10.309
$\nu$ $DOF$	11	12	12	13

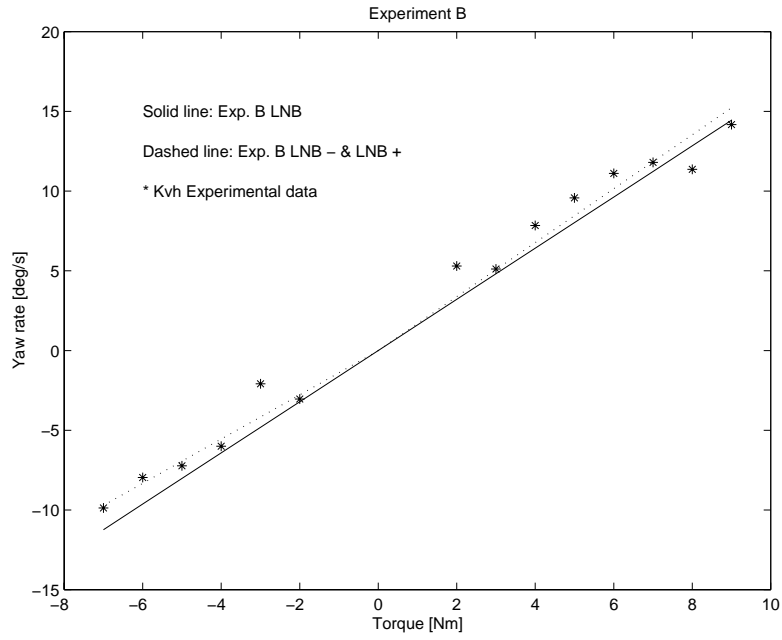
The parameter variances have been calculated by equation (4.6) having the torque variance been estimated by equation (4.12). The above reported tables are quite significant to understand the most correct way of modelling a pure yaw motion at standard operating velocities: the high value of the percentile relative error of the quadratic drag term indicates that at the considered velocities ( $\psi \leq 10$  deg /s) drag is a linear function of speed. This is also confirmed by the value of the quadratic drag term itself, that is



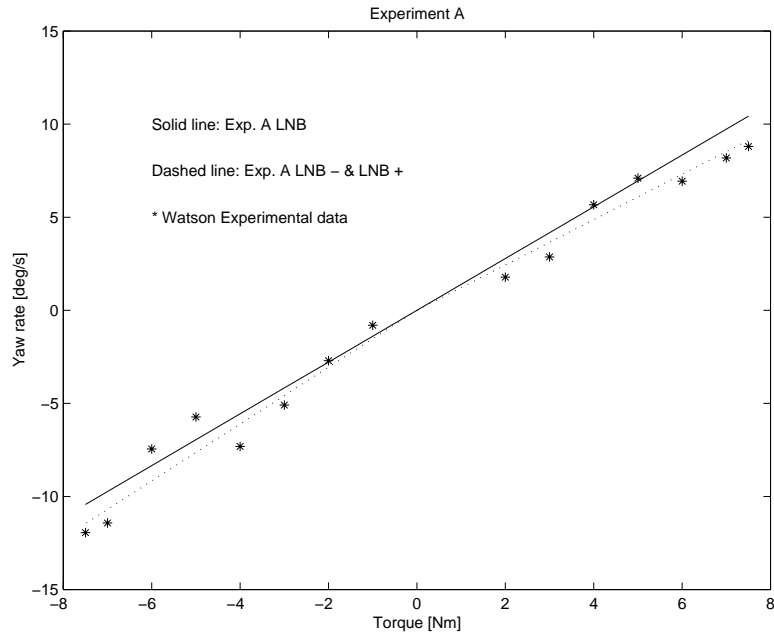
4.19. Yaw rate as a function of applied torque: experiment A, Kvh data

sometimes estimated to be negative, and more intuitively by the plots in figures (4.19) to (4.22). The bias term, introduced to model eventual unmodeled terms, is actually unnecessary as confirmed by the value of its estimated relative percentile error, and the most reliable model is the simple linear no-bias LNB one. The quadratic drag term is expected to become relevant only at higher yaw rates. The plots in figures (4.19), (4.20), (4.21) and (4.22) show also that modeling the right hand side and left hand side turns with different drag coefficients gives only a small fitting improvement that, for the sake of simplicity, can be neglected without serious loss of information.

At last the efficiency loss due to propeller hull and propeller propeller interactions has been considered: propeller hull interactions can be reasonably thought to be responsible of thruster efficiency loss in the B experiment. With reference to figure (4.3) the applied torque and yaw rate relative to the operation of the only front left (FL) and rear right (RR) thrusters are denoted by  $\tau_+$  and  $\psi_+$ : notice that when only the FL and RR thrusters apply a right turn torque there is no propeller propeller interaction with the rear left (RL) or front right (FR) thrusters and the outgoing water flow does not interact with the vehicles hull. As a consequence the efficiency of the two operating thrusters is assumed to be equal to the one measured in the thrust tunnel. On the contrary, when the same FL and RR thrusters apply a left hand side yaw rate, i.e.  $\psi_-$ , their efficiency is reasonably thought to be reduced by a propeller-hull interaction due to the thruster disposition. As



4.20. Yaw rate as a function of applied torque: experiment B, Kvh data



4.21. Yaw rate as a function of applied torque: experiment A, Watson data